Structural properties of granular Pd_xC_{1-x} films

A. Carl,* G. Dumpich, and E. F. Wassermann
Tieftemperaturphysik, Universität Duisburg, 47057 Duisburg 1, Federal Republic of Germany
(Received 3 December 1993)

We report on detailed and systematic investigations of the structural properties of thin ($t < 32$ nm) granular Pd_xC_{1-x} films with $0.1 < x < 0.5$, where x is the metal volume fraction. The films are prepared by coevaporation of palladium (Pd) and carbon (C) onto quartz- and NaCl-crystal substrates at room temperature in an uhv system. Since carbon is known to be insoluble in palladium within the whole composition region, we obtain granular Pd_xC_{1-x} films retaining their typical granular structure upon large variations of the metal volume fraction x. As revealed from transmission electron microscopic (TEM) investigations, granular Pd_xC_{1-x} films with $x < 0.3$ consist of mainly isolated small Pd clusters with mean diameters Φ of a few nanometers embedded in an amorphous carbon matrix. With increasing x clusters progressively coagulate, until at a certain metal volume fraction $x_p = 0.3$—which is the so-called percolation threshold—an infinite percolative network exists throughout the entire sample. From the analysis of TEM micrographs, we obtain size distributions for both cluster diameter Φ and cluster separation s for various films with different x, from which we obtain *mean* values as well as *typical* values for Φ and s with respect to the metal volume fraction x. This offers a *quantitative* comparison of the structural properties of a *real* granular system with that of a simple cubic model, often proposed being appropriate to describe the structural properties of granular systems.

I. INTRODUCTION

The electrical, optical, and magnetic properties of granular thin films are of long-standing interest in solid-state physics,[1] since—due to their inhomogeneous film structure—granular films exhibit rather interesting and different behavior as compared to structurally homogeneous bulk systems. Renewed interest in granular systems has arisen from recent experimental findings that granular *metallic* systems–like Co/Cu or Co/Ag–have been shown to also exhibit "giant" magnetoresistance effects[2]—similar to what is found for the case of magnetic multilayer systems.[3]

In the past, most experimental work has been attributed to granular systems consisting of two insoluble components, one of which being *metallic* the other *insulating*, like Ni-SiO_2, Pt-SiO_2, Au-Al_2O_3, or W-Al_2O_3, which were prepared by coevaporation as well as cosputtering.[4] In general, the structural properties of various granular systems are rather similar, and their physical properties systematically depend on the metal volume fraction x, which can be controlled experimentally by means of different evaporation rates during sample preparation. For metal volume fractions $x < x_p$, where x_p is the so-called percolation threshold, granular films are built up from mostly disconnected small metallic clusters with a rather narrow size distribution embedded in an electrically insulating matrix. Usually, mean cluster diameters are roughly < 10 nm. With increasing metal volume fraction, clusters progressively coagulate, until at a certain metal volume fraction $x = x_p$ an infinite percolative network exists throughout the entire sample. However, films with $x \approx x_p$ also consist of a certain amount of single clusters being isolated within the matrix, the number of which decreases with increasing x. Granular films with $x > x_p$ then consist of metallic clusters that are connected by small metallic bottlenecks, the number and lateral size of which increases with increasing x.

Correspondingly, the physical properties of granular systems strongly differ in varying the metal volume fraction from below x_p to above x_p. While, in general, films with $x > x_p$ show bulklike behavior,[5] on the other hand single-particle effects show up in various physical properties for films with $x < x_p$, resulting in, e.g., superparamagnetism for granular films consisting of mainly isolated ferromagnetic clusters like Fe/SiO_2 (Refs. 5 and 6) and quantum-size effects due to the small size of single clusters.[7] Although in the past most experimental as well as theoretical work has been attributed to the electrical-transport properties of granular systems, investigating both the nature of the metal-insulator transition at x_p (Refs. 8–13) and the temperature dependence of the dc conductivity,[4,14–25] within some generality it is found from several other experimental investigations[1,5] that various physical quantities systematically depend on the metal volume fraction x, because they are related to mean values for both cluster diameter Φ and cluster separation s, which in turn strongly depend on the metal volume fraction x. It is, therefore, desirable to know the detailed variation of $\Phi(x)$ and $s(x)$. Indeed, $\Phi(x)$ is well known and in addition found to be similar in magnitude for various granular systems.[4] On the other hand, to our knowledge $s(x)$ has not been investigated experimentally from electron microscopy up to now. It is interesting to note that $s(x)$, in contrary to $\Phi(x)$, should be considerably different in magnitude for various granular systems. This is apparent, since although $\Phi(x)$ is nearly the same in all cases, values for x_p are rather different, ranging be-

TABLE I. Percolation threshold x_p for various granular systems prepared by different experimental methods.

System	x_p	Author	Ref.	Prepared by
Sn-Ar	0.26	Rohde and Micklitz	10	gas aggregation
Pd-C	0.3	This work		coevaporation
Bi-Kr	0.34	Weitzel, Schreyer, and Micklitz	11	gas aggregation
$Au-Al_2O_3$	0.4	Abeles and co-workers	4	cosputtering
$Pt-SiO_2$	0.4	Abeles and co-workers	4	cosputtering
$Pt-Al_2O_3$	0.42	Gilabert *et al.*	19	cosputtering
$W-Al_2O_3$	0.47	Abeles and co-workers	4	cosputtering
Al-Si	0.5	Inglis *et al.*	17	cosputtering
Al-Ge	0.55	Deutscher, Rappaport, and Ovadyahu	8	coevaporation
$CoSiO_2$	0.5–0.6	Barzilai *et al.*	15	cosputtering
$Au-SiO_2$	0.54–0.62	McAlister, Inglis, and Kayll	18	cosputtering
$NiSiO_2$	0.6	Abeles and co-workers	4	cosputtering
$Cu-SiO_2$	0.6–0.65	Savvides *et al.*	16	cosputtering

tween $0.26 < x_p < 0.65$, as can be seen from Table I. Due to the lack of knowing $s(x)$, the structural properties of *real* granular systems are, therefore, often modeled by, e.g., a simple cubic arrangement of metallic clusters of equal size embedded in an insulating matrix equidistantly.[26] The question is, whether this model is more than just a first approximation, yielding reliable values for $s(x)$.

We have investigated in detail the structural properties of granular Pd_xC_{1-x} films with $0.1 < x < 1$ using transmission electron microscopy (TEM). In this paper we will restrict ourselves on films with $0.1 \leq x \leq 0.45$, close to the percolation threshold x_p, but with both $x < x_p$ and $x > x_p$. From size distributions for cluster diameter Φ as well as cluster separation s, obtained from electron micrographs for various films with different metal volume fractions x, we examine mean values (Φ, s) as well as standard deviations (σ_ϕ, σ_s) with respect to x. This allows us to compare the structural properties of our *real* granular system with that of a simple cubic model. Furthermore, it is shown that the behavior of standard deviations (σ_Φ, σ_s) versus x provides information on the position of the percolation threshold x_p for the Pd_xC_{1-x} system.

II. EXPERIMENT

Granular Pd_xC_{1-x} films with metal volume fraction $0.1 < x < 1$ and thicknesses $t < 32$ nm have been prepared by coevaporation of high-purity palladium (99.999%) and high-purity carbon (less than 0.1-at. % impurity concentration) simultaneously onto different substrates at room temperature in an uhv system ($p_0 < 10^{-7}$ Pa). Palladium (Pd) is evaporated by means of an electron-beam source and carbon (C) is sublimated from a resistively heated thin carbon rod. By using different evaporation rates for Pd and C, we are able to prepare Pd_xC_{1-x} films with various compositions and film thicknesses. The deposition of Pd and C is independently monitored by two separate quartz-oscillator balances, which are calibrated by optical interferometry (Tolansky). From this, we obtain the total film thickness $t = t_{Pd} + t_C$ and metal volume fraction $x = t_{Pd}/(t_{Pd} + t_C)$ with an accuracy of $\Delta x = \pm 5 \times 10^{-3}$. In each run, Pd_xC_{1-x} films with fixed composition are deposited onto NaCl and quartz substrates. The films deposited onto a cleaved NaCl substrate are removed afterwards in deionized water and transferred onto a small Cu net for TEM investigations, carried out with a Philips CM 12 (120 kV).

III. RESULTS AND ANALYSIS

As a typical example, Fig. 1 shows an electron micrograph of a granular Pd_xC_{1-x} film with $x = 0.22$ and total film thickness $t = 12.5$ nm. Since Pd and C are completely insoluble into each other,[27] the film consists of small spherical Pd clusters (dark areas), the mean diameter of which is around $\bar{\Phi} \approx 3$ nm, embedded in an amorphous carbon matrix (light areas). (Further on, *mean* values are indicated with a dash on top.) Most of the Pd clusters in Fig. 1 are disconnected by small carbon bridges, resulting in that the film belongs to the region of below the percolation threshold x_p. However, Fig. 1 also shows a certain amount of clusters being structurally coupled by small bottlenecklike connections.

As mentioned in the beginning, our investigation is

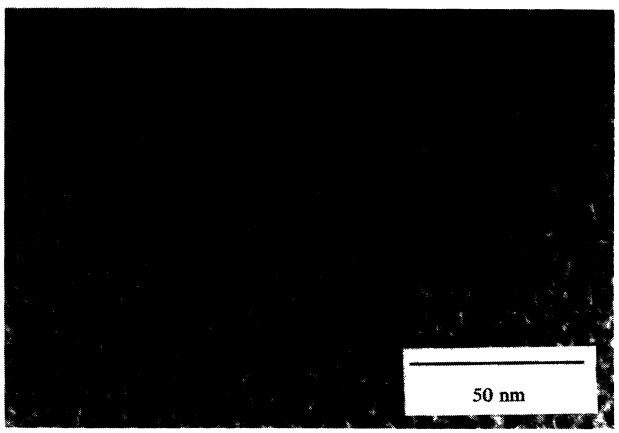

FIG. 1. Electron micrograph of a Pd_xC_{1-x} film with $x = 0.22$ and $t = 12.5$ nm.

aimed to determine (i) the percolation threshold x_p, as well as (ii) mean cluster diameters $\bar{\Phi}$, and (iii) mean cluster separations $\bar{s}$ *quantitatively* with respect to the metal volume fraction x. In a schematic representation, Fig. 2 shows the structural properties of our granular Pd_xC_{1-x} films, revealing both disconnected as well as connected Pd clusters, simply given as circles of equal size in Fig. 2. As indicated in Fig. 2, we have measured from TEM micrographs (i) the cluster diameter Φ and (ii) the cluster center-to-center (CTC) distance R, which is further on denoted CTC distance R. From the corresponding *mean* values $(\bar{\Phi},\bar{R})$, we have then calculated the *mean* cluster separation $\bar{s}$ for various films from $\bar{s}=\bar{R}-\bar{\Phi}$. This is indeed justified as will be shown below.

As is obvious from Fig. 1, cluster diameters Φ can easily be measured from TEM micrographs. On the other hand, if we like to measure cluster separations, we have to take into consideration that from TEM micrographs we can only measure values for R that are projected onto the "film surface." Therefore, measured values for R may be smaller as compared to real values for R if the film thickness t is larger than the mean cluster diameter $\bar{\Phi}$. In order to determine the magnitude of this discrepancy δR, we have investigated various films with the same metal volume fraction x but different total film thicknesses $t>\bar{\Phi}$ and $t\approx\bar{\Phi}$. We find mean values for R being nearly independent on t for films with $t>\bar{\Phi}$ and $t\approx\bar{\Phi}$, which means that also δR is independent on t. Moreover, for films with $t\approx\bar{\Phi}$, we may then extrapolate to the real two-dimensional case $(\bar{\Phi}=t)$ in order to examine the magnitude of δR in absolute values. For this we have measured the "real" and "projected" values of R, using a simple model, where spheres of typical (measured) diameters are arranged in different heights within a film of $t\approx\bar{\Phi}$. From this, we obtain the *typical* error δR in absolute magnitude with 0.5 nm $<\delta R<0.8$ nm. It turns out that these values of δR are smaller or at least equal as compared to σ_R, which is the standard deviation of $\bar{R}$ within our analysis (see below), proving that we are able to determine reliable data for $\bar{R}$.

For each film, mean values for cluster diameter $\bar{\Phi}$ and cluster CTC distance $\bar{R}$ are obtained from counting and measuring up to $N=1000$ data for both Φ and R from TEM micrographs, using an electronic measuring device providing a measuring accuracy of 0.05 nm. In order to check whether mean values $\bar{\Phi}$ and $\bar{R}$ are identical with most probable values for Φ and R, respectively, we also investigated the corresponding probability distributions for cluster diameters $N(\Phi)$ and cluster CTC distances $N(R)$. For that we have divided the range within $0<\Phi$, $R<10$ nm into 40 intervals of width $\Delta\Phi=\Delta R=0.2$ nm, into which data for Φ and R were attached, corresponding to their frequency $[N(\Phi), N(R)]$.

In Fig. 3, we present typical probability distributions $N(\Phi)$ (●) and $N(R)$ (○) for a Pd_xC_{1-x} film with $x=0.22$, as shown in Fig. 1. The dot size signifies the widths $\Delta\Phi$ and ΔR of intervals. As one can see from Fig. 3, $N(\Phi)$ and $N(R)$ are both symmetrical with respect to their most probable values Φ and R. Therefore, we have fitted $N(\Phi)$ as well as $N(R)$ by *Gaussian* distribution functions $N(\Phi,\bar{\Phi},\sigma_\phi)$ and $N(R,\bar{R},\sigma_R)$. Obviously, this provides an excellent fit to our data (solid lines in Fig. 3), from which we obtain mean values $(\bar{\Phi},\bar{R})$ along with corresponding standard deviations (σ_Φ,σ_R). For the film with $x=0.22$ shown in Fig. 1, the best fit gives $\bar{\Phi}=3.27\pm0.59$ nm and $\bar{R}=4.77\pm0.83$ nm. Also, for our other films, both $N(\Phi)$ and $N(R)$ nicely obey *Gaussian* distribution functions similar to what is shown in Fig. 3. The corresponding data for mean values $(\bar{\Phi},\bar{R})$ and standard deviations (σ_Φ,σ_R) are given in Table II for various films with $0.1\le x\le0.45$ together with data for x and film thickness t.

In earlier experimental work Granqvist and Buhrmann[28] found that $N(\Phi)$ is always of *log-normal* type for various granular systems, in what means that the

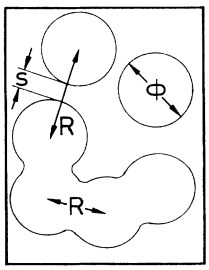

FIG. 2. Schematic presentation of the structural properties of granular Pd_xC_{1-x} films, revealing disconnected as well as connected clusters within the carbon matrix. The indicated quantities Φ and R are measured from TEM micrographs with Φ being the cluster diameter and R the cluster center-to-center distance, where the cluster separation s is calculated from $s=R-\Phi$.

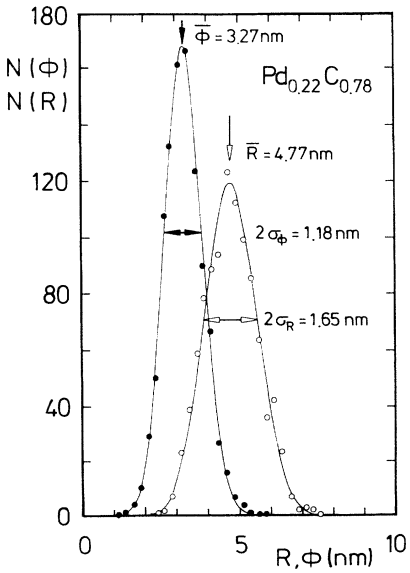

FIG. 3. Probability distribution $N(\Phi)$ (●) and $N(R)$ (○) for cluster diameter and cluster center-to-center distance, respectively, for the Pd_xC_{1-x} film with $x=0.22$, shown in Fig. 1. The solid lines correspond to fits from a *Gaussian* distribution function to the data from which mean values (Φ,R) as well as standard deviations (σ_ϕ,σ_R) are obtained.

TABLE II. x is the metal volume fraction, t the total film thickness, $\bar{\Phi}$ the mean cluster diameter, σ_Φ the standard variation of $\bar{\Phi}$, $\bar{R}$ the mean center-to-center distance, σ_R the standard variation of $\bar{R}$, $\bar{s}$ the mean cluster separation obtained from $\bar{s}=\bar{R}-\bar{\Phi}$, σ_s is the standard variation for $\bar{S}$ obtained from $\sigma_s=\sigma_\Phi+\sigma_R$.

x	t (nm)	$\bar{\Phi}$ (nm)	$\pm\sigma_\Phi$ (nm)	$\bar{R}$ (nm)	$\pm\sigma_R$ (nm)	$\bar{S}$ (nm)	$\pm\sigma_S$ (nm)
0.450	25.70	5.50	1				
0.400	26.60	3.87	0.73	4.10	0.70	0.23	1.43
0.350	11.20	4.75	0.58	5.37	0.72	0.62	1.30
0.340	21.20	3.93	0.60	4.54	0.65	0.61	1.25
0.333	27.00	3.02	0.58	4.03	0.74	1.01	1.32
0.320	28.10	2.82	0.40	3.84	0.60	1.02	1
0.315	21.60	3.13	0.57	4.49	0.73	1.36	1.30
0.310	5.80	3.35	0.65	4.59	1	1.24	1.65
0.304	27.29	3.94	0.64	5.03	0.92	1.09	1.56
0.303	8.90	3.83	0.80	5.24	1.15	1.41	1.95
0.220	12.50	3.27	0.59	4.77	0.83	1.50	1.42
0.200	13.80	1.71	0.35	3.21	0.49	1.50	0.84
0.190	18.50	3.45	0.60	5.17	0.79	1.72	1.39
0.180	7.70	1.73	0.30	3.27	0.40	1.54	0.70
0.100	22.40	2.69	0.78	4.99	1	2.30	1.78

logarithms of particle diameters reveal a Gaussian distribution. We have no indication for that, except for films with $x\approx 0.1$, which may also be analyzed using *log-normal* distributions (LND) for both $N(\Phi)$ and $N(R)$. However, here the standard deviation of the LND always equals $\sigma\approx 1$ so that $N(\Phi)$ and $N(R)$ for these films again may likewise be analyzed by a normal Gaussian distribution function.

From all measured data (Φ_i, R_i where $i=1,\ldots,N$) for each film we have then calculated $s_i=R_i-\Phi_i$, which in turn were attached to intervals of width $\Delta s=0.375$ nm within the range -5 nm $<s<5$ nm. From this, we obtain the probability distribution $N(s)$ for cluster separations s. A typical result is given in Fig. 4, which shows $N(s)$ for the same Pd_xC_{1-x} film with $x=0.22$ in Fig. 1. As one can see from Fig. 4, $N(s)$ is likewise symmetrical with respect to the mean value $\bar{s}$, giving rise to an excellent fit from a Gaussian distribution function $N(s,\bar{s},\sigma_s)$ to the data (solid line in Fig. 4). From the best fit, we obtain $\bar{s}=1.5\pm 1$ nm. It is important to note that we find the result for $N(s)$ in Fig. 4 being *independent* of any permutation of the data (Φ_i,R_i). Thus, mean values $\bar{\Phi}$ and $\bar{R}$ are statistically independent. This in turn then allows us to calculate the *mean* cluster separation $\bar{s}$ from mean values $\bar{s}=\bar{R}-\bar{\Phi}$. Indeed, using the corresponding *mean* values ($\bar{\Phi}=3.27\pm 0.59$ nm and $\bar{R}=4.77\pm 0.83$ nm) for the film with $x=0.22$ in Fig. 3, we obtain $\bar{S}=\bar{R}-\bar{\Phi}=1.5+1.42$ nm, which is equal in magnitude as compared to $\bar{S}=1.5\pm 1$ nm obtained from the maximum of $N(s)$ in Fig. 4. However, the standard deviation $\sigma_s=\pm 1.42$ nm calculated from $\sigma_s=\sigma_\Phi+\sigma_R$ is slightly larger than $\sigma_s=1$ nm as obtained from a fit of a Gaussian distribution function to $N(s)$. In the following we therefore consider $\sigma_s=\sigma_\Phi+\sigma_R$ as being the maximum error for $\bar{s}$ within our analysis, synonymous with the *typical* range of cluster separations $\bar{s}\pm\sigma_s$ within our films. For all Pd_xC_{1-x} films within $0.1\le x\le 0.45$, the structural properties were investigated in the same manner, as is demonstrated for the film with $x=0.22$ above. Values for $\bar{s}$ and σ_s are given in Table II.

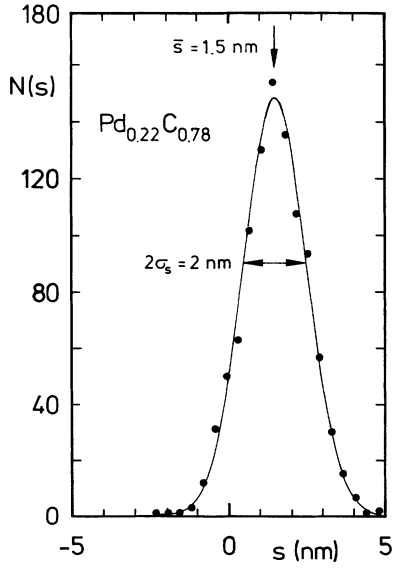

FIG. 4. Probability distribution $N(S)$ (●) for cluster separation for the Pd_xC_{1-x} film with $x=0.22$, shown in Fig. 1. The solid line corresponds to a fit from a *Gaussian* distribution function to the data from which we obtain the mean cluster separation with standard deviation σ_S.

IV. DISCUSSION

First, we like to analyze the behavior of σ_Φ and σ_R — given in Table II—with respect to the metal volume fraction x. In doing so, we have to take into account that both σ_Φ and σ_R not only depend on x but predominantly on the total number N of clusters counted. (It turns out

that this is at least the case for $N < 500$.) As mentioned above, however, N differs in magnitude within our analysis ranging between $100 < N < 1000$ for various films, thus making it inappropriate to study independently the behavior of σ_R and σ_Φ with x. On the other hand, since for each single film the total number of $N(\Phi)$ equals the number of $N(R)$, we may, therefore, investigate a *normalized* quantity, like σ_R/σ_Φ, with respect to x in order to compare the data for all our films.

In Fig. 5 we have plotted σ_R/σ_Φ versus metal volume fraction x within $0 < x < 0.4$. The error bars in Fig. 5 result from the possible variation for σ_Φ and σ_R itself, while fitting Gaussian distribution functions to $N(\Phi)$ and $N(R)$. The solid line may serve as a guide to the eye. According to our interpretation, σ_R/σ_Φ reveals a maximum at around $x \approx 0.3$, the exact position of which cannot be determined accurately in our case, because of the lack of experimental data in the range $0.22 < x < 0.3$. However, with emphasis towards the "diverging" branch of σ_R/σ_Φ for $x > 0.3$, we suggest that the maximum is located close to $x = 0.3$. It is now interesting to note that we find from simple inspection of TEM micrographs—taken for various films with different x—the position of the percolation threshold indeed close to the maximum of σ_R/σ_Φ within $0.3 < x_p < 0.315$ as indicated in Fig. 5 by the shaded area. This in turn means that the maximum in σ_R/σ_Φ versus x marks the position of the percolation threshold x_p for our granular Pd_xC_{1-x} system, pointing out that the analysis of probability distributions $N(\Phi)$ and $N(R)$ may provide a method to examine the percolation threshold x_p for granular systems. To prove this suggestion, more experimental work for various other granular systems and also theoretical work would be beneficial.

In Fig. 6 we have plotted the mean cluster diameter $\bar{\Phi}$ (full dots) with corresponding standard deviation σ_Φ (vertical lines) versus metal volume fraction x for various

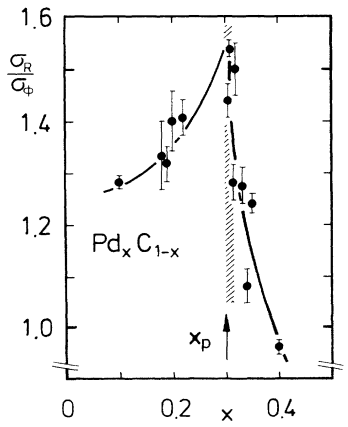

FIG. 5. The ratio σ_R/σ_Φ vs metal volume fraction x within $0.1 < x < 0.4$ for various granular Pd_xC_{1-x} films, exhibiting a maximum at the percolation threshold x_p, which is indicated by an arrow at $x_p = 0.3$. The solid line only serves as a guide to the eye. The shaded area within $0.3 < x < 0.315$ indicates the position of the percolation threshold as obtained from comparing TEM micrographs for various films with different x.

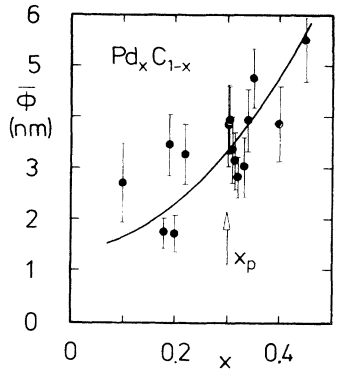

FIG. 6. Mean cluster diameters $\bar{\Phi}$ vs metal volume fraction x for various granular Pd_xC_{1-x} films within $0.1 < x < 0.45$ (full dots). The vertical lines represent the corresponding standard variation. The solid line indicates the average $\bar{\Phi}(x)$ behavior as a guide to the eye.

Pd_xC_{1-x} films within $0.1 \leq x \leq 0.45$. The solid line in Fig. 6 is a guide to the eye, representing the *average* $\bar{\Phi}(x)$ behavior on which we will refer below. Additionally, the position of the percolation threshold x_p is marked with an arrow at $x_p = 0.3$. It is striking that x_p does not show up from the experimental data in Fig. 6. Instead, $\bar{\Phi}(x)$ simply decreases with decreasing x within roughly 2 nm $< \bar{\Phi} < 6$ nm for films with $0.1 \leq x \leq 0.45$, as is indicated by the solid line.

In Fig. 7 we present the data for mean cluster separations $\bar{s}$ (full dots) versus metal volume fraction x for films with $0.1 \leq x \leq 0.4$. For each film, the vertical line indi-

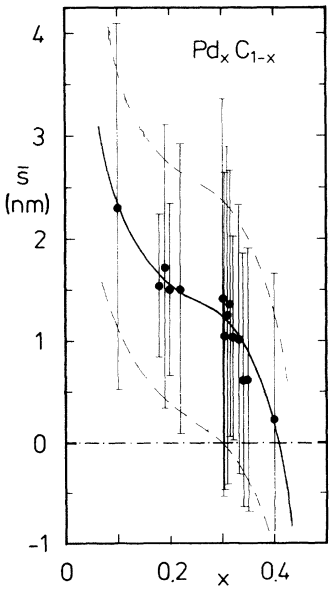

FIG. 7. Mean cluster separation $\bar{s}$ vs metal volume fraction x for various granular Pd_xC_{1-x} films within $0.1 < x < 0.4$ (full dots). The vertical lines represent the range of *typical* cluster separations within $\bar{s} \pm \sigma_s$, which are set off by the dashed lines. The *S*-shaped solid line may serve as a guide to the eye, emphasizing the overall $\bar{s}(x)$ behavior, whereas the dashed-dotted line marks the position of $\bar{s} = 0$.

cates the corresponding standard variation $\pm\sigma_s$. In the following we will identify the range of $\bar{s}\pm\sigma_s$ as being the regime of *typical* cluster separations, which is set off in Fig. 7 by dashed lines. The *S*-shaped solid line in Fig. 7 may again serve as a guide to the eye, emphasizing the overall $\bar{s}(x)$ behavior. The dashed-dotted line marks the position of $\bar{s}=0$. As is demonstrated in Fig. 7 by the solid line, $\bar{s}(x)$ only decreases with increasing x. This signifies that an increasing amount of Pd clusters grow together. From our results, given above, we know that the percolation threshold is located at $x_p=0.3$. However, as can be seen from Fig. 7 for films with $x\approx x_p$ the mean cluster separation is still $\bar{s}\approx 1.3$ nm >0. Instead we find $\bar{s}\to 0$ only for $x\approx 0.4$, which is definitely larger than x_p. This indicates that films with $0.3<x<0.4$ consist of a large amount of single clusters—in addition to the infinite percolative network—the number of which goes to zero for $x\to 0.4$. On the other hand, we may recognize two characteristic features in the vicinity of $x_p=0.3$ within Fig. 7. (i) For $x>0.3$, $\bar{s}$ decreases more rapidly with increasing x, resulting in the occurrence of the inflection point in the *S*-shaped $\bar{s}(x)$ behavior at $x\approx 0.3$. (ii) For films with $x\approx 0.3$ for the first time also *typical* cluster separations within the region $\bar{s}-\sigma_s$ become smaller than $\bar{s}=0$ with increasing x. This can be seen in Fig. 7 from the crossover of the dashed line with the dashed-dotted line at $x\approx 0.3$. These both may additionally indicate the position of the percolation threshold at $x_p=0.3$ in Fig. 7.

In Fig. 8 we have plotted the ratio $\bar{\Phi}/\bar{s}$ (full dots) versus metal volume fraction x for films with $0.1\le x\le 0.4$ from the experimental data for $\bar{\Phi}$ and $\bar{s}$ given in Table II. The full line is only a guide to the eye, however, consistent with the solid lines in Figs. 6 and 7, respectively. As one can see from Fig. 8, $\bar{\Phi}/\bar{s}$ strongly increases with increasing x. In the following, the behavior of $\bar{\Phi}/\bar{s}$ in Fig. 8 is compared with a model, where spheres of equal size Φ are embedded in an arbitrary matrix within a simple cubic arrangement. Such a model is often proposed being reasonable to describe the structural properties of real granular systems,[26] where the ratio Φ/s only depends on x with

$$\frac{\Phi}{S}=\left[\left[\frac{\pi}{6x}\right]^{1/3}-1\right]^{-1}. \tag{1}$$

The dashed line in Fig. 8 is calculated from Eq. (1) and shows substantially different behavior as compared to our experimental data. (i) Φ/s calculated from Eq. (1) partly differs in as much as 100% in magnitude from what is given from experiment (solid line) and (ii) Eq. (1) gives a percolation threshold located at $x_p^{sc}\approx 0.52$ which is roughly 70% larger than what is found from experiment in our case. Thus, we state that the underlying simple model yields only a rough approximation of the structural properties of a real granular system, whereas our investigation provides a *quantitative* determination of $\bar{s}(x)$. To prove this, future experimental work investigating the structural properties of various other granular systems and in particular the behavior of $\bar{s}(x)$ would be beneficial.

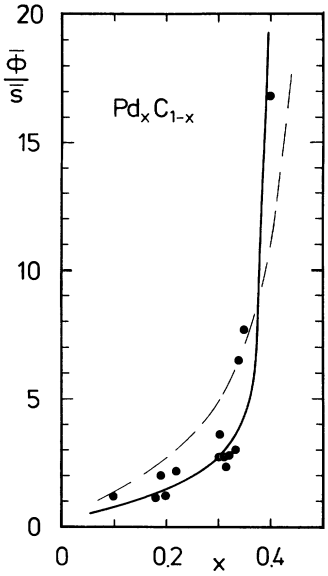

FIG. 8. The ratio $\bar{\Phi}/\bar{s}$ vs metal volume fraction x within $0.1<x<0.4$ The full dots are obtained from experimental data for $\bar{\Phi}$ and $\bar{s}$ given in Table II and the solid line is a guide to the eye, consistent with the solid lines in Figs. 6 and 7, respectively. The dashed line is calculated from Eq. (1) corresponding to the behavior of Φ/s for a model, where spheres of equal size are arranged with simple cubic symmetry.

V. SUMMARY

We have presented experimental results of a systematic investigation of the structural properties of thin granular Pd_xC_{1-x} films with metal volume fractions $0.1\le x\le 0.45$, carried out with TEM. From the analysis of TEM micrographs, we obtain size distributions for cluster diameter $N(\Phi)$ and cluster separation $N(s)$ for various films with different x. From a fit of Gaussian distribution functions to both $N(\Phi)$ and $N(s)$, we examine *mean* values as well as *typical* values for Φ and s with respect to x. It is suggested that the behavior of standard deviations for cluster diameters and distances with x provides information upon the position of the percolation threshold at $x_p\approx 0.3$ for our Pd_xC_{1-x} system. The analysis of $\bar{\Phi}(x)$ and $\bar{s}(x)$ allows us to compare the structural properties of a *real* granular system with that of a simple model often used to describe the structural properties of granular systems, where spheres of equal size are arranged with simple cubic symmetry. As is shown from the experimental data, this model is at least questionable in describing the structural properties of *real* granular systems.

ACKNOWLEDGMENTS

One of us (A.C.) wishes to thank the Alexander von Humboldt-Foundation (AvH), Bonn, Germany, for financial support.

*Present address: IBM Research Division, Almaden Research Center, 650 Harry Road, San Jose, CA 95120-6099.

[1]For a review see *Physical Phenomena in Granular Materials,* edited by G. D. Cody, T. H. Geballe, and P. Sheng, MRS Symposia Proceedings No. 195 (Materials Research Society, Pittsburgh, 1990).

[2]J. Q. Xiao, J. S. Jiang, and C. L. Chien, Phys. Rev. Lett. **68**, 3749 (1992); S. S. P. Parkin, R. F. C. Farrow, T. A. Rabedeau, R. F. Marks, G. R. Harp, Q. Lam, C. Chappert, M. F. Toney, R. Savoy, and R. Geiss, Europhys. Lett. **22** (6), 455 (1993).

[3]G. Binasch, P. Grünberg, F. Saurenbach, and W. Zinn, Phys. Rev. B **39**, 4828 (1989).

[4]B. Abeles, Ping Sheng, M. D. Coutts, and Y. Arie, Adv. Phys. **24**, 407 (1975); B. Abeles, H. L. Pinch, and J. I. Gittleman, Phys. Rev. Lett. **35**, 247 (1975).

[5]C. L. Chien, in *Science and Technology of Nanostructured Magnetic Materials,* edited by G. C. Hadjipanayis and G. A. Prinz (Plenum, New York, 1991).

[6]C. Laurent, D. Maurl, E. Kay, and S. S. P. Parkin, J. Appl. Phys **65**, 2017 (1989).

[7]W. P. Halperin, Rev. Mod. Phys. **58**, 553 (1986).

[8]G. Deutscher, M. Rappaport, and Z. Ovadyahu, Solid State Commun. **28**, 593 (1978).

[9]I. Balberg, N. Wagner, Y. Goldstein, and S. Z. Weisz, in *Physical Phenomena in Granular Materials* (Ref. 1), p. 233.

[10]M. Rohde and H. Micklitz, Phys. Rev. B **38**, 11 895 (1988); **36**, 7289 (1987).

[11]B. Weitzel, A. Schreyer, and H. Micklitz, Europhys. Lett. **12**, 123 (1990).

[12]Ch. Van Haesendonck and Y. Bruynseraede, Phys. Rev. B **33**, 1684 (1986).

[13]C. Vlekken, J. Vangrunderbeek, Ch. Van Haesendonck, and Y. Bruynseraede, *Proceedings of the International Symposium on Analogies in Optics and Microelectronics, Eindhoven, 1991* (North-Holland, Amsterdam, 1991).

[14]Ping Sheng, B. Abeles, and Y. Arie, Phys. Rev. Lett. **31**, 44 (1973).

[15]S. Barzilai, Y. Goldstein, I. Balberg, and J. S. Helman, Phys. Rev. B **23**, 1809 (1981).

[16]N. Savvides, S. P. McAlister, C. M. Hurd, and I. Shiozaki, Solid State Commun. **42**, 143 (1982).

[17]A. D. Inglis, J. R. Dutcher, N. Savvides, S. P. McAlister, and C. M. Hurd, Solid State Commun. **47**, 555 (1983).

[18]S. P. McAlister, A. D. Inglis, and P. M. Kayll, Phys. Rev. B **31**, 5113 (1985).

[19]A. Gilabert, M. Khatami, S. Berthier, J. Lafait, and P. Nédellec, Physica A **157**, 223 (1989).

[20]B. Weitzel and H. Micklitz, Phys. Rev. Lett. **66**, 385 (1991).

[21]A. M. Glukhov, N. Ya Fogel, and A. A. Shablo, Fiz. Tverd. Tela (Leningrad) **28**, 1043 (1986) [Sov. Phys. Solid State **28**, 583 (1986)]; T. Chui, G. Deutscher, P. Lindenfeld, and W. L. McLean, Phys. Rev. B **23**, 6172 (1981); G. Deutscher, B. Bandyopadhyay, T. Chui, P. Lindenfeld, W. L. McLean, and T. Worthington, Phys. Rev. Lett. **44**, 1150 (1980).

[22]S. P. McAlister, A. D. Inglis, and D. R. Kroeker, J. Phys. C **17**, L751 (1984)].

[23]A. G. Aronov, M. E. Gershenzon, and Yu. E. Zhuravlev, Zh. Eksp. Teor. Fiz. **87**, 971 (1984) [Sov. Phys. JETP **60**, 554 (1984)].

[24]Yoji Koike, Masami Okamura, and Tetsuo Fukase, J. Phys. Soc. Jpn. **54**, 3018 (1985).

[25]A. Carl, G. Dumpich, and D. Hallfarth, Phys. Rev. B **39**, 3015 (1989); **39**, 915 (1989); A. Carl, G. Dumpich, and E. F. Wassermann, Physica B **165&166**, 297 (1990).

[26]J. E. Morris, A. Mello, and C. J. Adkins, in *Physical Phenomena in Granular Materials* (Ref. 1), p. 181.

[27]Ernst Raub and Günter Falkenburg, Z. Metallk. **55**, 186 (1964).

[28]C. G. Granqvist and R. A. Buhrmann, J. Appl. Phys. **47**, 2200 (1976); **47**, 2220 (1976).

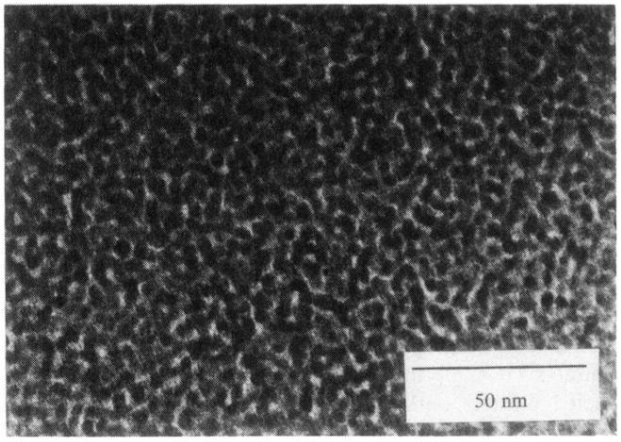

FIG. 1. Electron micrograph of a Pd_xC_{1-x} film with $x=0.22$ and $t=12.5$ nm.